# SMARTSAT
## COOPERATIVE RESEARCH CENTRE

# All-Weather Near Real-Time Monitoring of Bushfire with Satellite SAR

# All-Weather Near Real-Time Monitoring of Bushfire with Satellite SAR

**JULY 2023**

# Executive Summary

This executive summary overviews the project's objectives, progress, and challenges in developing a fully automated satellite Synthetic Aperture Radar (SAR) tool for bushfire detection and monitoring. The project agreement emphasizes the need for robust results, comprehensive case studies, and integration with existing operational systems.

The first objective is to develop a fully automated SAR-based bushfire detection and monitoring tool, which includes automatic satellite data acquisition, DInSAR processing, and burned area (BA) automatic detection. The project has made significant progress by automating and refining the pipeline using Sentinel-1A satellite. The developed pipeline delivers dependable outcomes round-the-clock through the utilization of SAR imagery, which has the ability to penetrate through clouds and smoke. This exceptional feature enables us to continuously monitor bushfire activity, thereby expediting quick and effective decision-making and response. However, challenges for detection accuracy arise due to variable topography, vegetation, and environmental conditions, and then consequently lead to mis-interpretation. Ensuring a consistent capture cadence with standardized imagery geometry parameters is crucial for improving the tool's performance.

The second objective entails conducting comprehensive case studies on bushfires during Australia's 2021-22 and 2022-23 fire seasons. The case studies, primarily focused on New South Wales (NSW), have integrated project activities with input and feedback from the NSW Rural Fire Services (RFS). The conducted studies illustrate how the project's work is pertinent to the operations of the NSW RFS. They also highlight the importance of utilizing multiple sources of imageries, including SAR and visible spectrum imageries, for processing techniques validation and fine-tuning, e.g. Sentinel-2, Himawari-8, and Landsat 8.

The third objective centres around understanding end-user use cases and exploring potential pathways for integrating the tool's outputs with existing operational systems. Through workshops and feedback sessions, the project has documented the requirements and expectations of end users, particularly the people from NSW RFS, who emphasize the need for near real-time responses to fires. The project outcomes represent a robust step towards meeting these objectives, but the current imagery capture frequency does not yet provide the necessary data for real-time operations.

The report highlights that while the project has made significant progress, additional time and potential technological advancements are needed to ensure a consistent supply of high-quality imagery. Improvements in imagery capture frequency and advances in processing techniques will be vital in achieving the project's primary and secondary objectives.

Overall, the project's objectives and progress demonstrate the importance of developing a fully automated SAR-based bushfire detection and monitoring tool. With continued research and development efforts, including addressing the challenges associated with image capture and interpretation, the project aims to provide a valuable solution that can significantly enhance bushfire management capabilities.

# Acronyms

BA (Burned Area)

DEAH (Digital Earth Australia Hotspot)

DInSAR (Differential Interferometric Synthetic Aperture Radar)

DP (Dual Polarization)

GEC (Geocoded Ellipsoid Corrected)

GEO (Geocoded Terrain Corrected)

GIS (Geographic Information System)

HR (Hazard Reduction)

ILC (Improved Luminance Contrast)

InSAR (Interferometric Synthetic Aperture Radar)

LC (Luminance Contrast)

MSR (Multi-Scale Retinex)

SAR (Synthetic Aperture Radar)

SICD (Sensor Independent Complex Data)

SLC (Single Look Complex)

# Contents

# 1 Introduction

Bushfires have long been a significant and recurring threat to Australia, exacerbated by the impacts of climate change. One of the most devastating bushfire seasons in recent history was the 2019-20 Australian bushfire season, commonly referred to as the Black Summer. During this period, we have witnessed an unprecedented outbreak of intense bushfires across various parts of Australia, starting in June 2019 and lasting until May 2020. The Black Summer bushfires resulted in widespread destruction, with over 9,352 buildings destroyed and a tragic loss of life, including 34 direct deaths and 417 indirect deaths caused by bushfire smoke inhalation.

In response to the escalating threat of bushfires and their increasingly severe impacts, this project aims to harness the potential of high-resolution satellite Synthetic Aperture Radar (SAR) imageries by exploiting its interferometric coherence. The primary objective is to develop a reliable and early detection system for bushfires that can operate day and night in all weather conditions, significantly enhancing bushfire management capabilities.

The project encompasses a range of activities, including the establishment of a robust satellite SAR-based production line. This production line will enable the conversion of remote-sensing imagery into valuable fire intelligence. The project's outcomes include the development of an innovative tool based on satellite SAR technology. This tool will utilize Sentinel-1 SAR satellites images. It will be designed to seamlessly integrate into existing bushfire information systems, such as the Digital Earth Australia Hotspot (DEAH) system. Furthermore, the project will produce case studies detailing the application of the newly developed tool in detecting and monitoring bushfires during the 2019-2021 and 2022-2023 fire seasons.

In addition to the technical advancements, the project will culminate in a comprehensive report presenting the lessons learned and recommendations for future follow-on project phases. This report will be formulated based on insights and feedback gathered from a group of emergency services clients assembled during workshops conducted by the project. The collective expertise and input from industry stakeholders will contribute to shaping the direction and potential expansion of the project in subsequent phases.

By leveraging the interferometric coherence of high-resolution satellite SAR imagery, this project aims to revolutionize the early detection and monitoring of bushfires. The envisioned outcomes promise an innovative tool that can enhance existing bushfire information systems, provide valuable insights for fire management agencies, and offer significant potential for future advancements in bushfire prevention and response.

# 2 Case Studies

## 2.1 Dataset

The case study of this project utilised a comprehensive dataset of five different fire events, providing valuable insights into the effectiveness and potential of SAR imagery for bushfire detection and monitoring. Table 1 presents an overview of the fire events in the dataset, highlighting the diversity of scenarios and the range of challenges encountered.

TABLE 1 FIRE EVENTS DATASET

| Fire Name | State | Ignition Date | Containment Date |
|-----------|-------|---------------|------------------|
| Kangaroo Ridge | NSW | 09/10/2020 | 18/10/2020 |
| Royal National Park Artillery Hill | NSW | 12/05/2020 | 15/05/2020 |
| Wattamolla | NSW | 22/04/2021 | 03/05/2021 |
| Mt Mitchell | NSW | 28/04/2020 | 05/05/2020 |
| Green Wattle Creek | NSW | 26/11/2019 | 09/02/2020 |
| Alpha Road | NSW | 06/02/2023 | 22/03/2023 |

Three satellite platforms were utilised to capture the SAR imagery: Sentinel-1, ALOS-2, and Capella. Each satellite offers unique capabilities and imaging parameters, as illustrated in Table 2. Leveraging multiple satellites allowed for a broader coverage of the fire events and facilitated the examination of the consistency and accuracy of the SAR-derived information across different platforms.

TABLE 2 SATELLITE PARAMETERS

| | Sentinel-1 | ALOS-2 | Capella |
|---|-----------|--------|---------|
| Band Type | SAR - C Band | SAR – L Band | SAR -X Band |
| Wavelength (cm) | 5.6 cm | 24.2cm | 3.1 cm |
| Polarisation | VH, VV | HH, HV | HH |
| Resolution (m) | 10 | 10 | 0.3 |
| Product | SLC | Fine[10m] DP | GEO |

Including multiple fire events within the dataset enabled a comprehensive analysis of SAR imagery's performance in various geographical contexts, fire intensities, and vegetation types. The diversity of fire events ensured that the findings derived from the case study are representative and applicable to a wide range of real-world scenarios.

## 2.2 Methodology

### 2.2.1 Automatic satellite data acquisition system

The parameters for download software are shown in Table 3.

TABLE 3 PARAMETERS FOR DOWNLOAD SOFTWARE

| Parameters | Geographic Coordination 1 | Ingestion Period | Product Type | Query Result Format | Storage Path | Estimated Download Time |
|---|---|---|---|---|---|---|
| Sample Case | --latmin -34 <br> --latmax -33 <br> --lonmin 150 --lonmax 151 | -d 20220201 -f 20220301 | SLC | XML | /RawData | 40mins |

The account information will be stored in the apihub.txt first. With the geographic coordinate and the ingestion period specified, the query result will be stored in XML format, and download results will be saved in the pre-configured path. The time cost is mainly dependent on network download speed. The command for sample case should be like this shown on the screen: python Sentinel_download.py -a apihub.txt -w Data -d 20220201 -f 20220301 --latmin -34 --latmax -33 --lonmin 150 --lonmax 151 -s S1A*SLC)

### 2.2.2 Automatic DInSAR process system

The coherence algorithm of SAR is based on the product of SAR radar images. It measures the correlation between the radar backscatter signals reflected from the same location over different acquisitions. By comparing the phase information of the radar echoes, the coherence algorithm calculates the degree of similarity or consistency between the radar images. Given two SAR images $\mathbf{I}_1$ and $\mathbf{I}_2$ at times $t = 1, 2$, we can calculate the interferometric coherence by

$$\gamma = \frac{\mathbb{E}[\mathbf{I}_1 \mathbf{I}_2^*]}{\sqrt{\mathbb{E}[|\mathbf{I}_1|^2] \mathbb{E}[|\mathbf{I}_2|^2]}} \tag{1}$$

where $\mathbf{I}_t^*$ is the complex conjugate of $\mathbf{I}_t$, $\mathbb{E}[\cdot]$ denotes the expectancy value. The interferometric coherence is able to measure changes between SAR pair (Zebker and Villasenor 1992). We obtained coherence results for two SAR images based on this equation.

This part includes three steps: data pre-process, DInSAR process and raster merge process.

Data pre-process integrates several open-source algorithm functions from GMTSAR (Sandwell, David et al. 2011), including align_top.csh, p2p_S1_TOP.csh, etc. It takes a long time, about 20-40 minutes. Data in the three formats including mth, par, r00, and other information can be generated, which are necessary inputs for the next step.

Differential Interferometric Synthetic Aperture Radar (DInSAR) process is an in-house program fully developed and maintained by UNSW-GEOS Group. Execute the automated python script, this program will call the C++-based processing function to perform DInSAR processing on the pre-processed data. Processing time is approximately 15-30 minutes.

The function of raster merge process is to merge three rasters into one output. Based on the processing results of DInSAR, the third step is to execute an automated python script to merge multiple rasters into a complete image. The coherence difference result can be used for band composition with optical images. The fusion result can strengthen the features and optimize the recognition algorithm. Processing time is within 1 minute.

All the three steps are integrated together into a Docker, which can be suitable for any operating system. The benefits of Docker in building and deploying applications are many:

1. Caching a cluster of containers

2. Flexible resource sharing

3. Scalability - many containers can be placed in a single host

4. Running your service on hardware that is much cheaper than standard servers

5. Fast deployment, ease of creating new instances, and faster migrations.

6. Ease of moving and maintaining your applications

7. Better security, less access needed to work with the code running inside containers, and fewer software dependencies

The overall time cost is shown in Table 4.

TABLE 4 AUTOMATIC DINSAR PROCESS SYSTEM

| Parameters | Data pre-process | DInSAR process | Raster merge process | Overall |
|---|---|---|---|---|
| Time cost (min) | 20-40 | 15-30 | 1 | 36-71 |

### 2.2.3   Burned Area (BA) Automatic Detection

This section comprises two components: the difference operation process and the BAauto_detection process. Of which, the second step is our key process, which is an in-house algorithm for detecting burned scars based on the coherence difference results.

**Difference operation process:** Coherence results for the fire event including pre-event pair and co-event pair will be generated based on DInSAR process. In order to remove signals of decorrelation from waterbody and vegetation, reduce disturbance from buildings and highlight the burned scars, the difference operator will be executed and hence the coherence difference image will be generated. According to (Ge, Wang et al. 2021), other disturbances would be further suppressed to single out burned scars if we calculate the difference between coherence images from the co-event pair and pre-event pair to generate the coherence difference image.

**BAauto_detection process:** In the previous section, a coherence difference image has been formed to highlight the burned areas. However, due to the properties of SAR data, there are still a lot of speckle noise and false alarms in the coherence difference image, and the continuous burned area seems to be split. It is necessary to propose an improved algorithm to express the "visual difference" so that the coherence difference image has the autonomous capability to help us focus on the burned areas. This concept is inherited from the filtering mechanism of the human brain and can be used to target the salient change areas.

Having conducted numerous experiments, we found that existing saliency detection algorithms were not suitable for our coherence difference images. As a result, we introduced the Improved Luminance Contrast (ILC) algorithm as a proposed solution. The original Luminance Contrast (LC) method was first proposed by Zhai et. al (Zhai and Shah 2006) and can be used to get the global contrast of each pixel in the entire image. When directly applying it to the coherence difference image, the speckle noise and split

burned pieces will dominate with high contrast. Therefore, we need to filter out the part of speckle noise and connect the split burned patches before employing a visual saliency algorithm.

We employ Multi-Scale Retinex (MSR) algorithm (Rahman, Jobson et al. 1996) to carry out the image enhancement, which also means suppressing the noise and improving the image's visual effect. It can be expressed as

$$R'(x,y) = \sum_{i=1}^{n} \omega_i\{\log S(x,y) - \log[F_i(x,y) * S(x,y)]\} \tag{2}$$

where $n$ is the number of scales being used, and we set $n = 3$ in our experiments. The $\omega_i$ are the weighting factors for the scales, and $\omega_1 + \omega_2 + \omega_3 = 1$. $S(x,y) = R(x,y)L(x,y)$, $R(x,y)$ and $L(x,y)$ denote the low and high-frequency components of the image, respectively. $F_i(x,y)$ are the surround functions given by $M_n(x,y) = K_n \exp\left[-(x^2 + y^2)/\sigma_n^2\right]$, where the $K_n$ are selected so that $\iint F(x,y)dxdy = 1$. In our study, we use Gaussian functions as the surround functions and set $\sigma_1 = 5$, $\sigma_2 = 80$, $\sigma_3 = 200$.

Then, the key step is to connect the split burned pieces to generate the continuous burned scar and eliminate the unrealistic false scar. The opening operation from morphology could be employed to achieve this goal. It can be operated by $(A\ominus S) \oplus S$, where $\ominus$ and $\oplus$ denote the Erosion and Dilation operations, respectively, and the $S$ is the operation template ($5 \times 5$ pixels). After we carry out the opening operation many times after MSR, the small space between the burned pieces can be mostly eliminated. The iteration parameter is crucial as it may have a huge and immediate impact on the final result, and we set iterations = 30 in our study. Different results based on different iterations will be shown in the next section.

Finally, we calculate the visual saliency map by

$$\text{SalS}(a_m) = \sum_{n=0}^{255} f_n\|a_m - a_n\|. \tag{3}$$

Given the input image obtained after opening operations, the grayscale value of each pixel $a_i$ is known. Let $a_n$ represents $n_{th}$ grayscale value level in $a$, $f_n$ denotes the frequency of $a_n$, and $\|a_m - a_n\|$ is the Euclidean distance between $a_m$ and $a_n$. Through the application of ILC algorithm, potential burned areas are targeted and highlighted with stronger visual contrast. We form a probability map according to the grayscale value level of pixels from the saliency map. In our experiments, we set the threshold as 0.58. The pixels of the probability map with values > 0.58 will be classified as burned, and the remaining pixels are classified as unburned. The framework for BA Automatic Detection is shown in Figure 1.
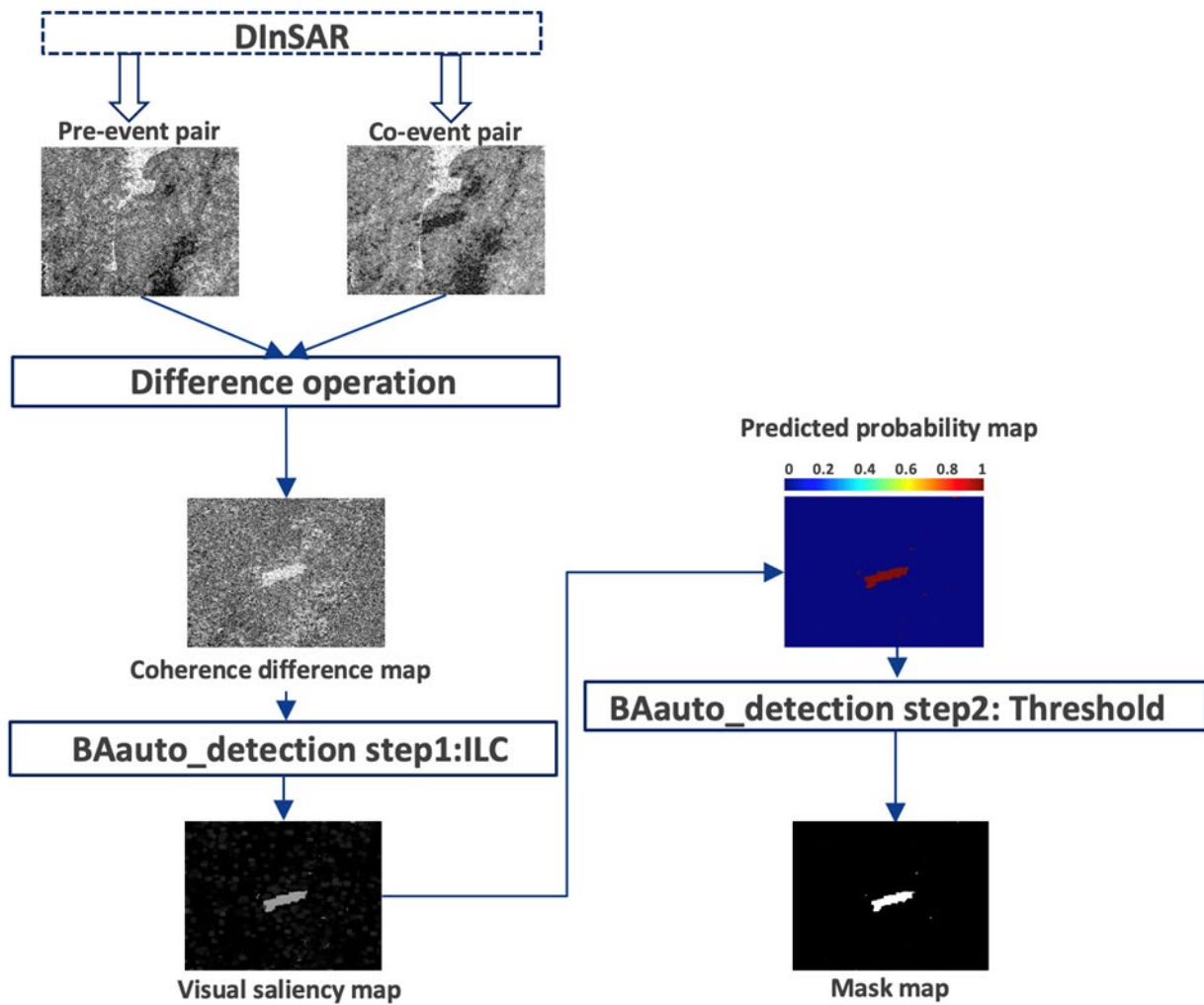
**Figure 1 The framework for BA Automatic detection**

## 2.3   Experimental Results

Figure 2 depicts the complete coverage map of the ALOS-2 coherence difference result. The red box highlights the specific locations of the five case studies conducted in this analysis. All the rough burned area shapefiles are provided by Digital Atlas Australia Beta (Commonwealth of Australia (Geoscience Australia), 2023). The focus of this study is on bushfires that occurred in New South Wales, Australia.

In the coverage map, both red and blue colours represent the degree of change. The red areas indicate significant coherence changes from October 2020 to October 2021, suggesting substantial alterations in the landscape during this period. Conversely, the blue areas represent significant coherence changes from October 2019 to October 2020, indicating notable changes in the preceding year. These changes in coherence are attributed to the impact of bushfires, which can cause extensive damage to vegetation and alter the landscape.
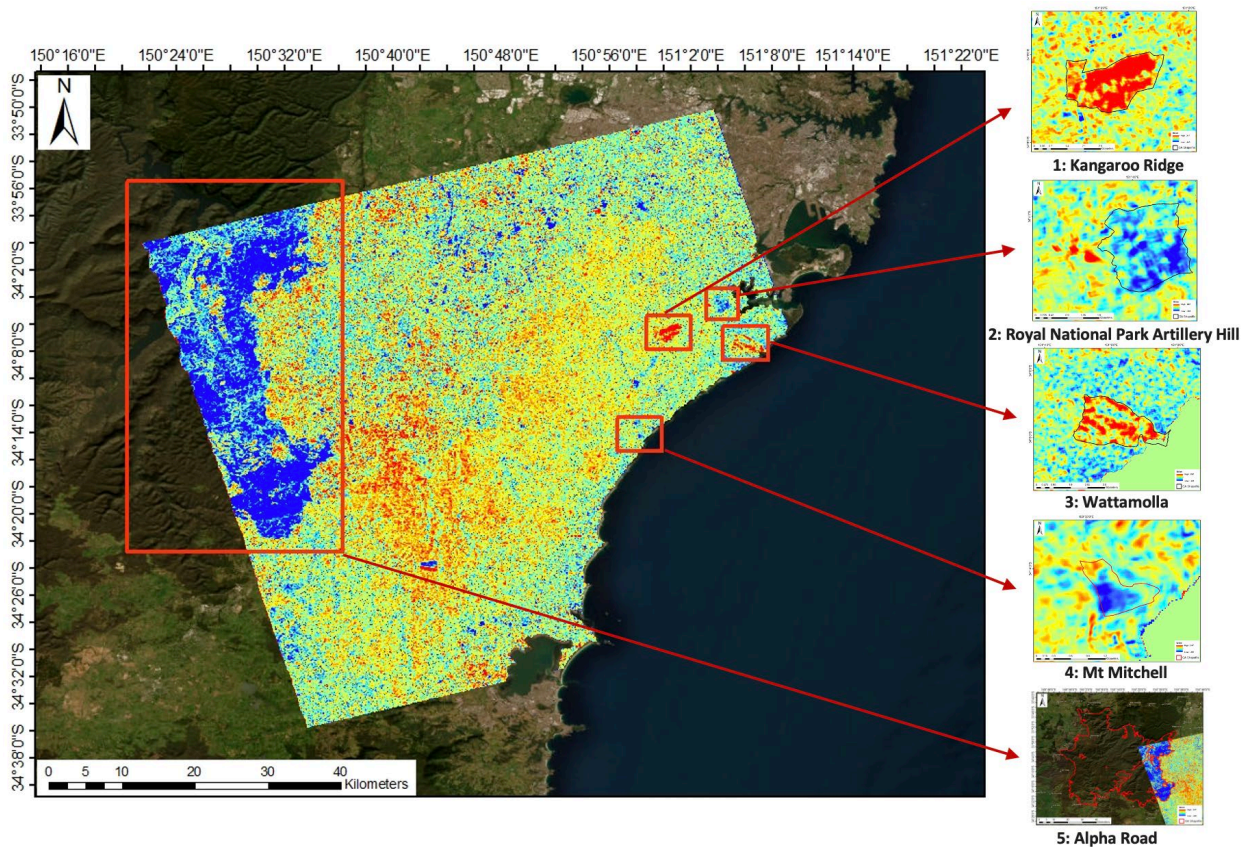
**Figure 2 Overview of ALOS-2 coherence difference image**

The coherence difference analysis employed in this study proves valuable for delineating burned areas resulting from bushfires. By quantifying the coherence changes over time, we can effectively identify regions that have experienced significant fire-related transformations. This information serves as a crucial foundation for further analysis and understanding of the bushfire impacts on the affected areas.

### 2.3.1 Kangaroo Ridge

The first fire event is known as Kangaroo Ridge Fire, which occurred in Waterfall from October 10 to October 18, 2020. We downloaded four SLC images from Sentinel-1 to form one pre-event pair and two co-event pairs. In addition to these, three ALOS-2 images are utilized to help test the potential of L-band SAR for burned area mapping. The timeline for SAR satellite data acquisition is shown in Figure 3.
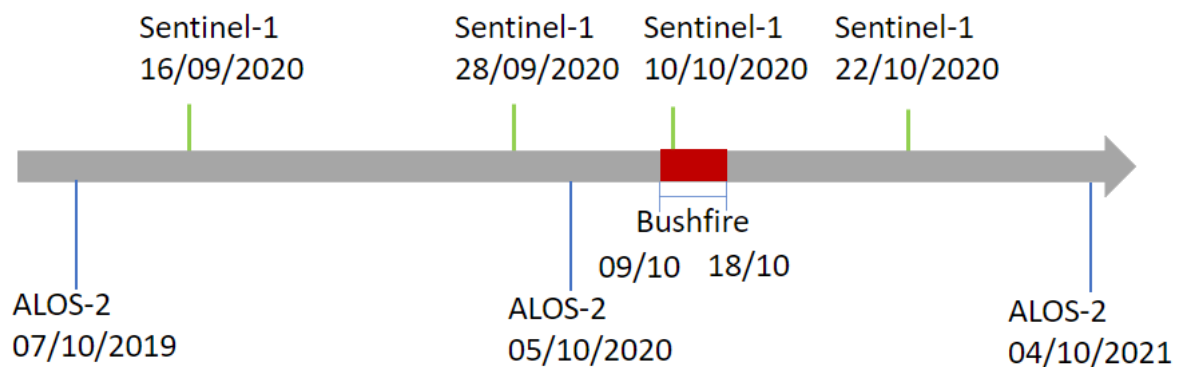


**Figure 3 Data acquisition timeline of SAR data for Kangaroo Ridge fire event**

Figure 4(a) visually represents the coherence differences between the pre-event and co-event pairs obtained from Sentinel-1 SAR imagery. The pre-event pair comprises two SAR images captured before the fire event, while the co-event pair includes two SAR images captured before and during the fire event. This coherence difference analysis provides valuable insights into the changes during the fire event and is a key indicator for detecting burn areas. By identifying areas of significant change, the coherence differences offer a foundation for further analysis and interpretation. Figure 4(b) showcases the saliency map generated from the coherence difference using the burn area (BA) detection algorithm. This saliency map effectively delineates the extent of the burn area, providing a clear and concise visualization of the affected regions. It serves as a crucial tool for identifying and quantifying the spatial distribution of the fire event, enabling accurate assessment and monitoring of the burned area. Figure 4(c) presents the mask map generated from the saliency map using a specific threshold (0.58*max-value). The mask map helps shape the burn area by highlighting the regions that exhibit the desired saliency level. This map can be further utilized for generating shapefiles, facilitating the integration of the burn area information into geographic information systems (GIS).



(a)  (b)  (c)
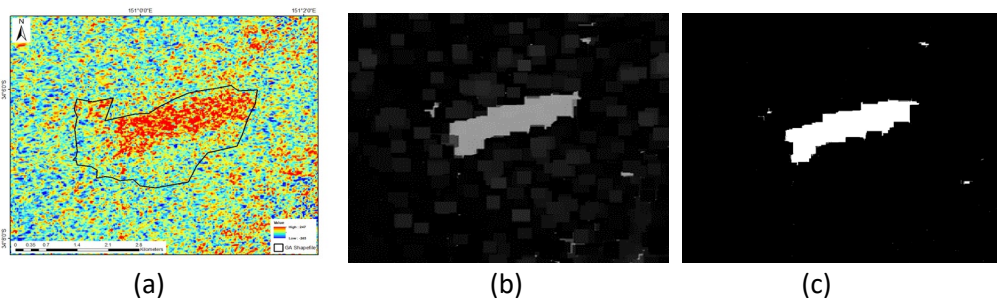
**Figure 4 The initial results from Sentinel-1 over Kangaroo Ridge fire area. (a) The initial coherence difference image obtained via the difference operator, (b) saliency map obtained via ICL algorithm, (c) mask map obtained by the specific threshold. (Black perimeter in (a) is obtained from Geoscience Australia (GA))**

To demonstrate the coherence difference's capability for monitoring the entire propagation process of a fire event, an image captured after the fire event was included to generate another co-event pair. The new coherence difference result (Figure 5(a)) was obtained using the same pre-event pair. However, it's important to note that due to the temporal decorrelation over two cycles (24 days), the coherence difference is significantly impacted by noise. As a result, detecting burned scars becomes more challenging, as the noise interferes with the image quality. Figures 5(b) and 5(c) illustrate the saliency and mask maps derived from this time series analysis.



(a)  (b)  (c)
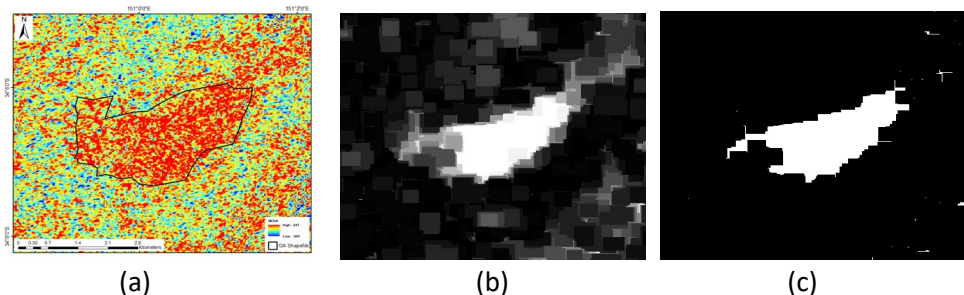
**Figure 5 The results from Sentinel-1 over Kangaroo Ridge fire area. (a) The coherence difference image obtained via the difference operator, (b) saliency map obtained via ICL algorithm, (c) mask map obtained by the specific threshold. (Black perimeter in (a) is obtained from GA.)**

Figure 6 shows a coherence difference map from ALOS-2 imagery, of which the time baseline is approximately one year, but the temporal decorrelation does not affect the singled-out process for the burned area detection, It can be seen that the disturbance compressed much more than Sentinel-1. It emphasized the penetration ability of L band SAR is much better that C band, which leads to better highlighting over the burned area.
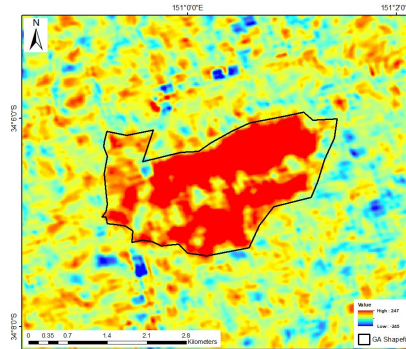


**Figure 6 The coherence difference image from ALOS-2 over Kangaroo Ridge fire area**

In addition to the SAR imagery analysis, four optical satellite images (shown in Figure 7) were utilized for validation and cross-comparison purposes. The optical satellite images included Sentinel-2, Himawari-8, and Landsat 8, each offering unique characteristics and capabilities. The Sentinel-2 imagery provides a high-resolution view with a revisit time of 5 days, enabling detailed examination of the affected areas at a 10-meter resolution. Himawari-8, with its high revisit time of 20 minutes, offers the advantage of quickly capturing fire events in near-real-time, although its resolution is lower at 2 kilometres. On the other hand, Landsat provides a moderate-resolution view with a revisit time of 16 days at a 30-meter resolution. Utilizing these optical satellite images allows for validation, comparison, and a comprehensive understanding of the fire event from different perspectives.



| (a) | (b) | (c) | (d) |
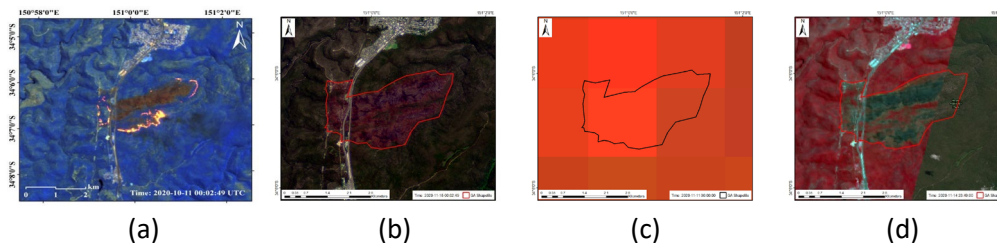
**Figure 7 The results from optical satellites over Kangaroo Ridge fire area. (a) The false-colour image (band 12, 11 and 8) from Sentinel-2 during fire event, (b) the true-colour image (band 4, 3 and 2) from Sentinel-2 after fire event, (c) the false-colour image (band 7, 4 and 1) from Himawari-8 during fire event, (d) the false-colour image (band 5, 4 and 3) from Landsat-8 after fire event. (Red or black perimeter is obtained from GA.)**

The coherence differences, saliency map, and mask map derived from the SAR analysis provide valuable information for accurately assessing and monitoring the burn area and its severity. The validation and cross-comparison with optical satellite images enhance the reliability and confidence in the derived results, ensuring a comprehensive understanding of the fire event.

It is worth noting that the case study results from Sentinel-1 and ALOS-2 align perfectly with the optical satellite imagery, while the shapefile provided by GA displays inaccuracies. This further emphasizes the efficacy of SAR imagery in accurately detecting and monitoring burn areas, highlighting its potential as a valuable tool in fire management and assessment.

### 2.3.2 Royal National Park Artillery Hill

The second fire event was about a prescribed burn, which occurred in Royal National Park Artillery Hill from May 12 to May 15, 2020. Three SLC images from Sentinel-1 were downloaded to form one pre-event pair and one co-event pair, and three same ALOS-2 images are utilized in this case to generate L-band coherence difference map. The timeline for SAR satellite data acquisition is shown in Figure 8.
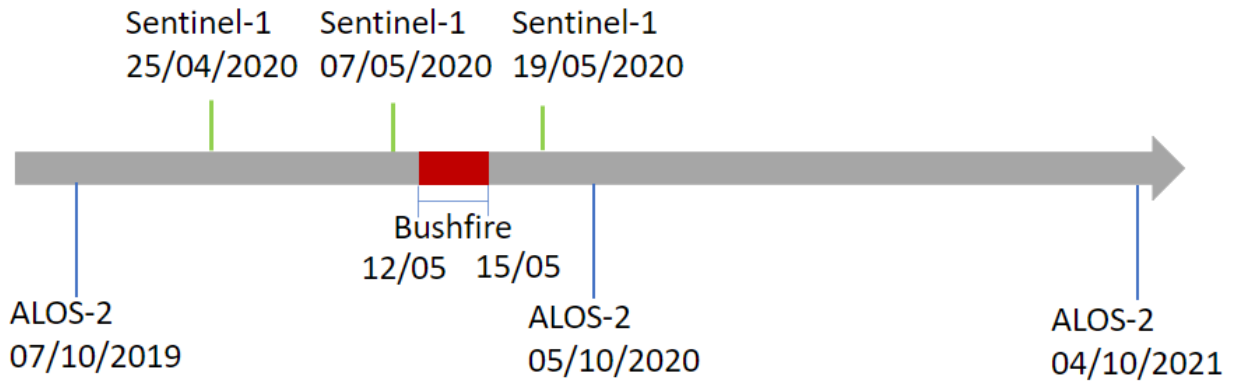


**Figure 8 Data acquisition timeline of SAR data for Royal National Park Artillery Hill fire event**

Figure 9 displays the coherence difference map, saliency map, and mask map generated from the project's product pipeline, respectively. Additionally, Figure 10 showcases the results obtained from ALOS-2 data. Our saliency maps indicate that the severity of the burned area is higher in the bottom right region, providing valuable insights into the spatial distribution of fire severity. Notably, the severity information is not available in the GA shapefile, highlighting the competitive advantage of our results in terms of providing comprehensive fire severity analysis.



|                 (a)                 |                 (b)                 |                 (c)                 |
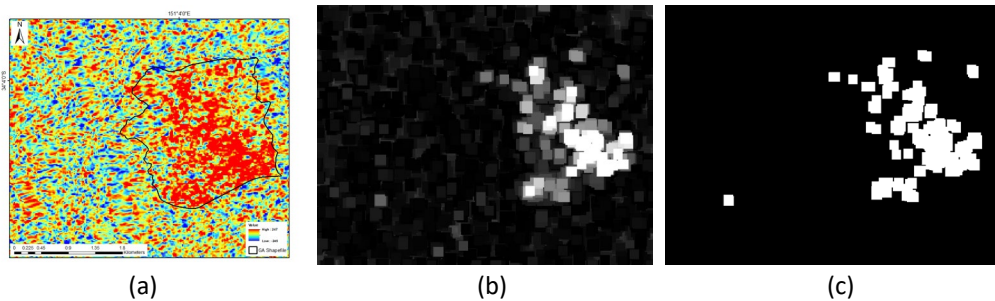
**Figure 9 The results from Sentinel-1 over Royal National Park Artillery Hill fire area. (a) The coherence difference image obtained via the difference operator, (b) saliency map obtained via ICL algorithm, (c) mask map obtained by the specific threshold. (Black perimeter in (a) is obtained from GA.)**
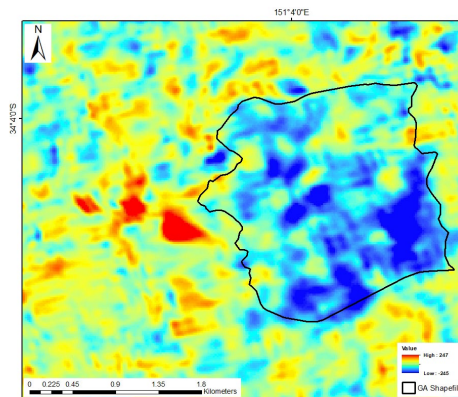
**Figure 10 The coherence difference image from ALOS-2 over Royal National Park Artillery Hill fire area**

To validate and cross-compare our findings, we employed three optical satellite images: Sentinel-2, Himawari-8, and Landsat 8, as shown in Figure 11. The Sentinel-2 false-color image, in particular, clearly validates our fire severity findings. The visual comparison between our derived results and the optical satellite image provides confidence in the accuracy and reliability of our analysis.



(a)　　　　　　(b)　　　　　　(c)　　　　　　(d)
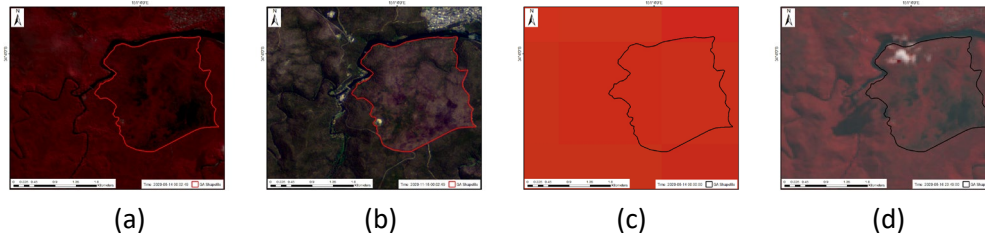
**Figure 11 The results from optical satellites over Royal National Park Artillery Hill fire area. (a) The false-colour image (band 8, 3 and 2) from Sentinel-2 during fire event, (b) the true-colour image (band 4, 3 and 2) from Sentinel-2 after fire event, (c) the false-colour image (band 7, 4 and 1) from Himawari-8 during fire event, (d) the false-colour image (band 5, 4 and 3) from Landsat-8 after fire event. (Red or black perimeter is obtained from GA.)**

### 2.3.3　Wattamolla

The Wattamolla fire event was also a Hazard Reduction (HR) burn, which happened from April 22 to May 3, 2021. Three SLC images from Sentinel-1 were downloaded to form one pre-event pair and one co-event pair. And three same ALOS-2 images are utilized in this case to generate L-band coherence difference map. The timeline for SAR satellite data acquisition is shown in Figure 12.
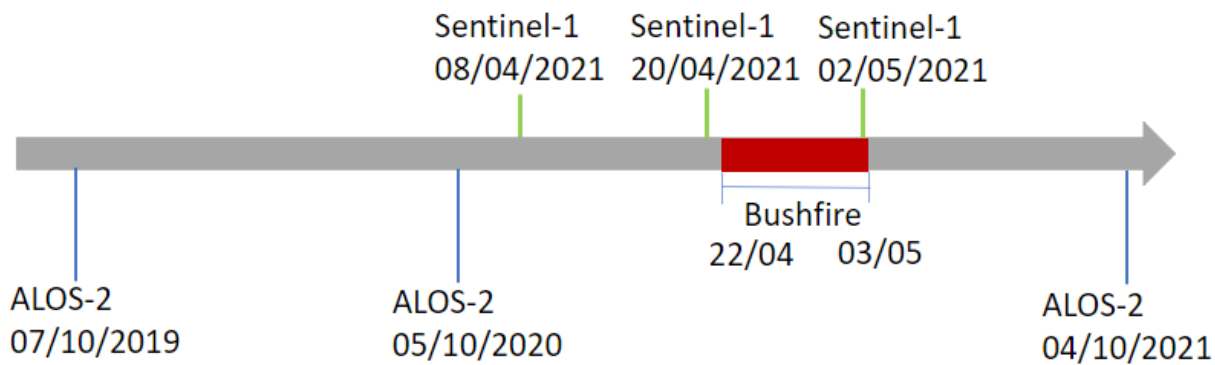


**Figure 12 Data acquisition timeline of SAR data for Wattamolla HR burn**

Figure 13 illustrates the coherence difference map, saliency map, and mask map generated from the project product pipeline, respectively. Figure 14 presents the result obtained from ALOS-2 data. It is worth noting that, within the extent of the Geoscience Australia (GA) shapefile, there is an area in our result that indicates it is not burned.

(a)                                (b)                                (c)

**Figure 13 The results from Sentinel-1 over Wattamolla Hazard Reduction burn area. (a) The coherence difference image obtained via the difference operator, (b) saliency map obtained via ICL algorithm, (c) mask map obtained by the specific threshold. (Black perimeter in (a) is obtained from GA.)**
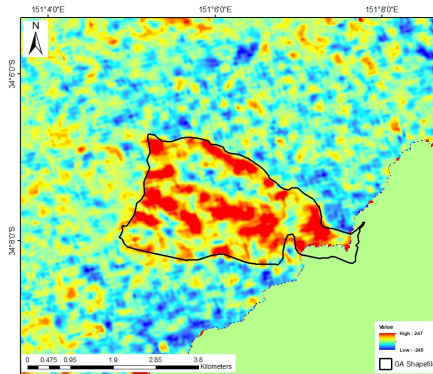


**Figure 14 The coherence difference image from ALOS-2 over Wattamolla Hazard Reduction burn area**

To validate and cross-compare our findings, three optical satellite images were utilized: Sentinel-2, Himawari-8, and Landsat 8,as shown in Figure 15. The optical images confirm our result by indicating that not all areas within the GA shapefile are burned. This observation suggests that the shapefile provided by GA may not represent the ground truth accurately.



(a)                                (b)                                (c)
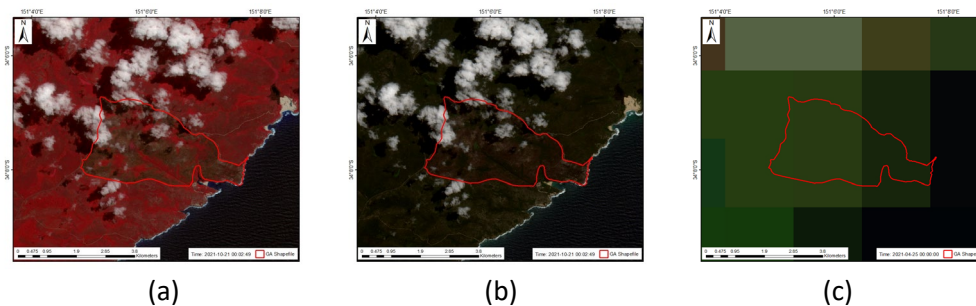
**Figure 15 The results from optical satellites over Wattamolla HR burn area. (a) The false-colour image (band 8, 3 and 2) from Sentinel-2 after fire event, (b) the true-colour image (band 4, 3 and 2) from Sentinel-2 after fire event, (c) the false-colour image (band 6, 4 and 3) from Himawari-8 during fire event. (Red perimeter is obtained from GA.)**

By comparing the SAR-derived maps with the optical satellite images, we gain valuable insights into the accuracy and reliability of our results. It is essential to consider these discrepancies and limitations in the GA shapefile when interpreting and analyzing the fire-affected areas. This case study highlights the significance of integrating different data sources, such as SAR and optical imagery, to enhance the understanding and validation of bushfire mapping outcomes.

### 2.3.4   Mt Mitchell

The Mt Mitchell prescribed burn happened from April 28 to May 5, 2020. Three SLC images from Sentinel-1 were downloaded to create one pre-event pair and one co-event pair. And three identical ALOS-2 images are used in this case study to form L-band coherence difference map. The timeline

illustrating the acquisition of SAR satellite data can be seen in the figure 16.
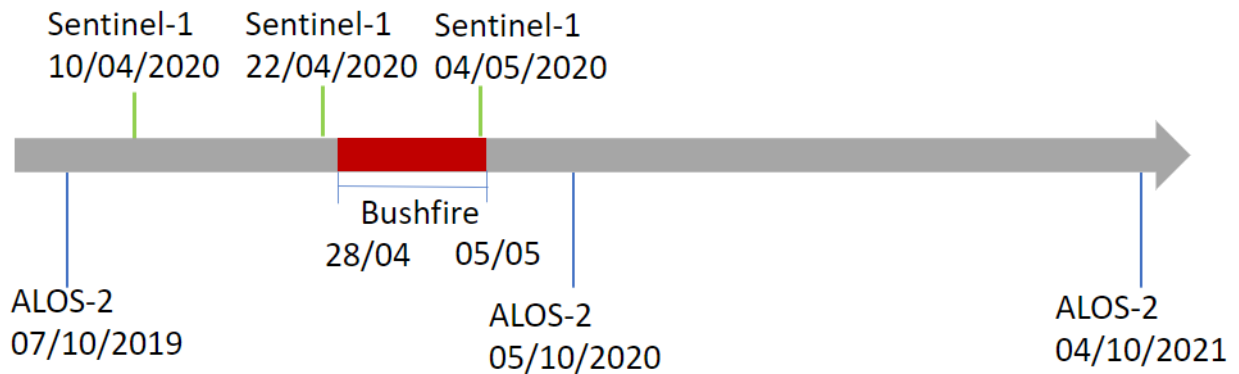


**Figure 16 Data acquisition timeline of SAR data for Mt Mitchell HR burn**

As depicted in Figure 17, the burned scars are not clearly highlighted in the coherence difference result obtained from Sentinel-1 imagery. Consequently, our algorithm cannot be applied in this particular case. However, the coherence difference result obtained from ALOS-2 data is deemed acceptable.



(a)                                    (b)                                    (c)
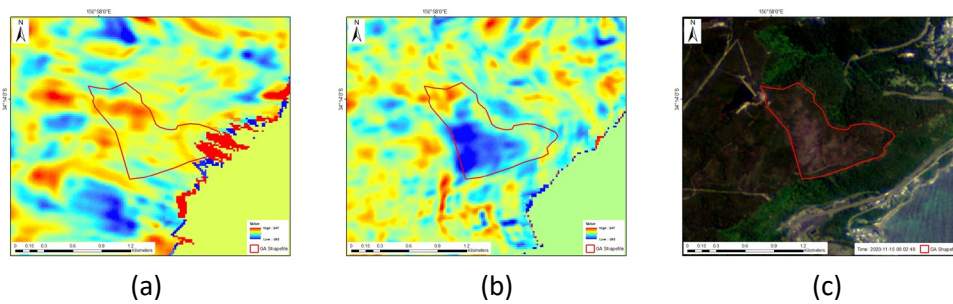
**Figure 17 The results from different satellites over Mt Mitchell HR burn area. (a) The coherence difference image from Sentinel-1 obtained via the difference operator, (b) the coherence difference image from ALOS-2 obtained via the difference operator, (c) the true-colour image (band 4, 3 and 2) from Sentinel-2 after fire event. (Red perimeter is obtained from GA.)**

Through comparison and validation with optical data from Sentinel-2 and the GA shapefile, it becomes evident that the coherence difference result from ALOS-2 is significantly superior to that from Sentinel-1. This finding emphasizes the crucial role of penetration ability in bushfire analysis cases. The ALOS-2 imagery's enhanced ability to penetrate through vegetation and capture detailed information contributes to more accurate and reliable bushfire mapping outcomes.

## 2.3.5   Green Wattle Creek

The Green Wattle Creek fire event was a big bushfire that persisted for several months. Similarly, three SLC images from Sentinel-1 were downloaded to create one pre-event pair and one co-event pair, while three identical ALOS-2 images are used to form L-band coherence difference map. The timeline illustrating the acquisition of SAR satellite data can be seen in the figure 18.
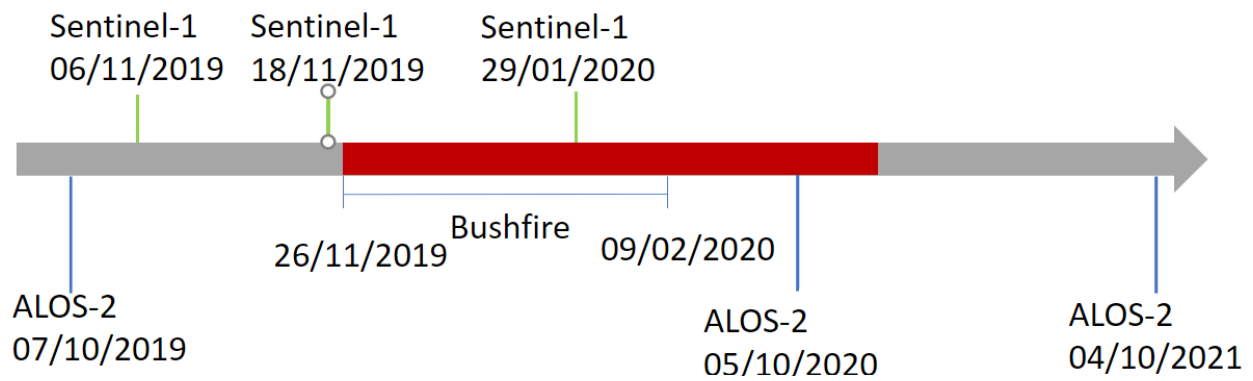
**Figure 18 Data acquisition timeline of SAR data for Green Wattle Creek fire event**

Figure 19(a) shows a coherence difference map from Sentinel-1 imagery, and Figure 19(b) shows a coherence difference map from ALOS-2 imagery. It can be seen that the result from Sentinel-1 is affected by several disturbances, including vegetation variation and wind-driven temporal decorrelation. Apart from that, the left bottom of the burned area boundary is delineated, which illustrates Sentinel SAR data's capabilities in burned area mapping. In addition, although limited to spatial coverage, the result from ALOS is competitive, which emphasizes again the band penetration ability is of great importance.



(a)                                                                                     (b)
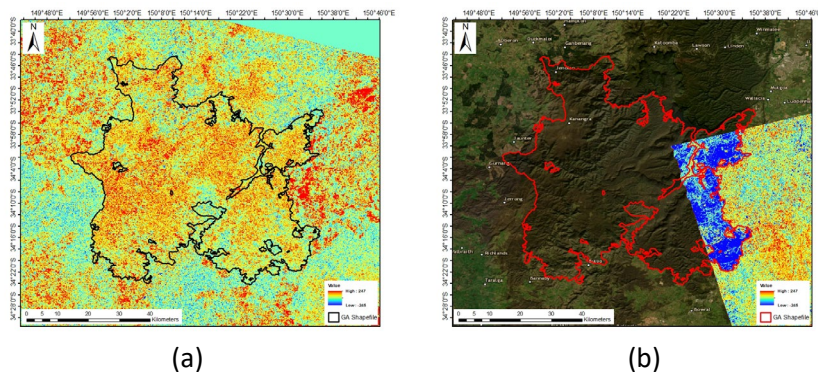
**Figure 19 The results from SAR satellites over Green Wattle Creek bushfire area. (a) The coherence difference image from Sentinel-1 obtained via the difference operator, (b) the coherence difference image from ALOS-2 obtained via the difference operator. (Black or red perimeter is obtained from GA.)**

Optical data from Sentinel-2 and Himawari-8 were employed for validation purposes, as depicted in Figure 20. However, it was determined that all the optical images were unsuitable for validation due to the prolonged duration of the fire event, which lasted for more than 3 months. This case study highlights an important lesson learned: for long-term bushfire events, a time-series-based analysis approach is more favourable and efficient. By leveraging time-series data, we can capture the temporal dynamics and spatial variability of the fire, enhancing our ability to monitor and manage such prolonged events effectively.

**Figure 20 The results from optical satellites over Green Wattle Creek bushfire area. (a) The false-colour image (band 8, 3 and 2) from Sentinel-2 during fire event, (b) the true-colour image (band 4, 3 and 2) from Sentinel-2 during fire event, (c) the false-colour image (band 6, 4 and 3) from Himawari-8 during fire event. (Red perimeter is obtained from GA.)**

### 2.3.6 Alpha Road

The Alpha Road fire event became an out of control bushfire first recorded on February 6, 2023, and contained on March 22, 2023. This case can help us test the capability of our system for near-real time bushfire mapping. Unfortunately, there is no available ALOS-2 data to generate L-band result during this fire period. Instead, X-band Capella data is used in this case. The details for Capella data source are illustrated in  table 5 and the timeline for SAR satellite data used can be seen in the figure 21.

TABLE 5 DETAILS FOR CAPELLA DATA SOURCE

| Time | Orbit State | Orbit Plane | Platform | Look direction | Look angle | Incidence angle | Polarization | Mode | Gec | Geo | SLC | SICD |
|------|------------|-------------|----------|----------------|-----------|-----------------|--------------|------|-----|-----|-----|------|
| 08/03/2023 | ascending | 97 | 7 | left | 37.5 | 41.1 | HH | Stripmap | | | | |
| 11/03/2023 | ascending | 97 | 8 | left | 36.3 | 39.7 | HH | Stripmap | ✓ | ✓ | ✓ | ✓ |
| 15/03/2023 | ascending | 97 | 8 | left | 38.3 | 42 | HH | Stripmap | | | | |
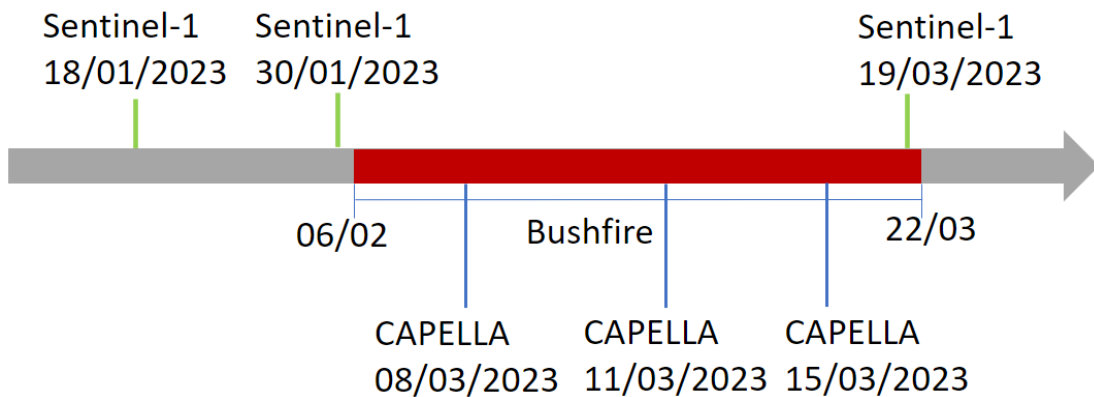


**Figure 21 Data acquisition timeline of SAR data for Alpha Road fire event**

For this case study, a near real-time bushfire mapping task was examined using Capella X-band SAR and Sentinel C-band SAR imagery. It is important to note that the X-band SAR has a lower penetration capability compared to the C-band SAR. Due to limitations arising from the look angle difference in the Capella data, coherence difference analysis was not feasible in this case. Instead, intensity difference was utilized as an alternative approach.

The preliminary result obtained from the Capella X-band SAR data captured on 08/03/2023 and 15/03/2023 is presented in Figure 22(a). The Capella team performed their change detection algorithm and obtained their result, as shown in Figure 22(b). Additionally, the result from the Sentinel C-band SAR

processed using the project pipeline is displayed in Figure 22(c). It is important to note that there have been four cycles between the co-event pair for the Sentinel 1 data, resulting in a significant mismatch caused by temporal decorrelation.



|  (a)  |  (b)  |  (c)  |
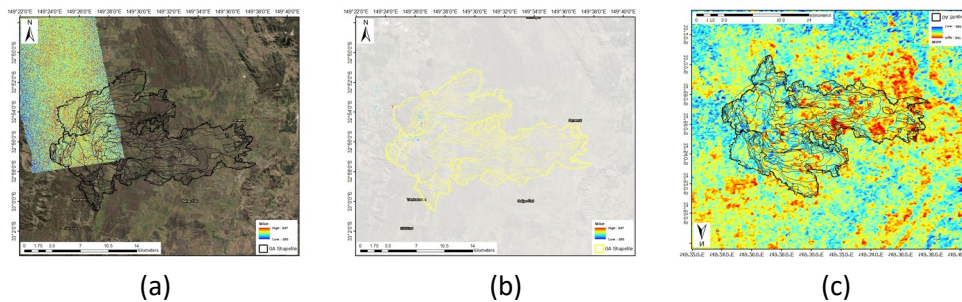
**Figure 22 The results from SAR satellites over Alpha Road fire area. (a) The intensity difference image obtained via the difference operator, (b) the change detection result obtained from Capella team, (c) the coherence difference image obtained via the difference operator. (Black or yellow perimeter is obtained from RFS.)**

To validate and cross-compare the results, false-colour images from Sentinel-2 and Himawari-8 were utilized, as depicted in Figure 23. Remarkably, the results align perfectly with the shapefile provided by GA. This observation emphasizes that the mapping capability of the X-band and C-band SAR for detecting burned areas is not optimal and suggests that future work should explore the use of L-band SAR, which is more favourable for this purpose.



|  (a)  |  (b)  |
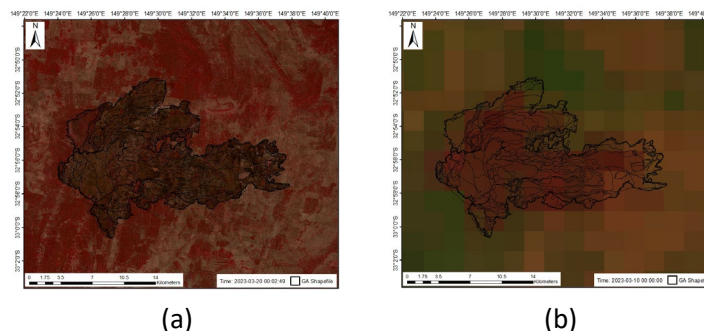
**Figure 23 The results from optical satellites over Alpha Road fire area. (a) The false-colour image (band 8, 3 and 2) from Sentinel-2 after fire event, (b) the false-colour image (band 6, 4 and 3) from Himawari-8 during fire event. (Black perimeter is obtained from RFS.)**

# 3  Discussion

The research has highlighted the significance of consistent capture geometry parameters, such as orbit plane, direction, look direction, and look angle, in obtaining reliable and accurate SAR imagery. The variable responses of SAR are influenced by changes in the incidence angles of the topography being captured, indicating the need for further research to account for topography and vegetation changes.

Throughout the project, several valuable lessons have been learned:

1) processing multiple source imagery is essential to meet the demands of near real-time responses to bushfires;

2) the integration and automation of processing components play a vital role in streamlining the workflow and ensuring efficient data analysis. Using mixed resolutions, considering both large and small-scale areas,

is crucial for effective detection and response. Containerisation of code has proven significant, enabling additional development and ensuring flexibility for future enhancements;

3) validating results is necessary for project development, allowing for agile responses and continuous improvement, and

4) the project has emphasized the importance of industry engagement as it promotes collaboration, fosters knowledge exchange, and supports the establishment of realistic expectations. By actively involving industry stakeholders, this project has benefited from their expertise and feedback, enhancing its overall success.

# 4   Conclusion

In conclusion, this project has demonstrated the potential of using SAR imagery for revolutionizing bushfire detection and monitoring. The insights gained and the lessons learned will serve as a foundation for further advancements in this field. By embracing lessons learned and exploring future opportunities, future projects can effectively leverage SAR technology to enhance fire management capabilities, minimize the impacts of bushfires, and protect vulnerable communities and ecosystems.

The project plan outlined a comprehensive approach to harnessing high-resolution satellite SAR imagery for bushfire detection and monitoring. The project objectives were achieved through post-event processing, and attempted near-real-time processing, with encouraging results, answering many research questions, and more that warrant additional research and development with future opportunities.

The post-event processing phase focused on ensuring the reliability and robustness of the bushfire detection and monitoring products. The team compared the results obtained from satellite InSAR coherence processing with data from aerial infrared scanning and in-field surveys to validate the performance of the newly developed system. Technical challenges were addressed, such as precise image matching, terrain effect correction, and classification and segmentation of coherence results. The phase also involved the conversion of bushfire intelligence from raster to vector format, enabling effective dissemination and end-user satisfaction.

The near real-time processing phase emphasized efficiency and automation throughout the end-to-end service chain. The team optimized computing efficiency to balance timeliness and product details. Down sampling products for significant bushfire events and exploring the use of dedicated local high-performance servers or cloud computing services were crucial considerations. The phase aimed to streamline the workflow and explore best practices for optimal computing efficiency.

The final end-user testing phase, led by Nova Systems, involved a user-centred design workshop in evaluating the satellite InSAR coherence-based products and the near-real-time system. The workshop engaged emergency services and management clients, including partnerships with NSW RFS, DPIE, and DEWLP organizations. The outputs were systematically reviewed for integration into operational systems and future projects.

The project plan facilitated collaboration with relevant agencies and industry partners. Agreements with ESA, CSIRO, GA, and RFS were sought to ensure the availability of SAR imagery, data processing, and integration with existing systems. The project team maintained regular communication through weekly meetings and monthly progress reports. An advisory panel provided strategic advice and guidance.

The deliverables of this project include a highly efficient software tool for satellite SAR-based bushfire detection and monitoring, as well as extensive case studies. The workshop with end users and industry partners described pathways for adopting and integrating the tool into operational systems. A loose-

integration approach, ensuring compatibility with existing bushfire information systems, appears to be the best measure of future implementations. Industry partners, such as Nova Systems, have the potential to embed the SAR capability within their existing industry systems. Cross-platform compatibility and comprehensive documentation are essential for seamless integration.

This project plan has provided a solid foundation for leveraging satellite SAR imagery to enhance bushfire detection and monitoring capabilities. The outcomes and insights gained from this project have the potential to revolutionize bushfire management practices, contribute to the safety of communities, and protect valuable ecosystems in Australia.

# 5    Future Opportunities

ALOS-2 imagery processing has exceeded the project team's previous best results, demonstrating the immense potential of leveraging multiple imagery sources for bushfire monitoring and response. The recognition that optimal outcomes were attained through the utilization of ALOS-2 imagery highlights the significance of obtaining and processing a wide range of datasets for a comprehensive understanding of bushfires. This discovery further underscores the importance of future opportunities to concentrate on the integration and processing of multiple source imagery, enabling near real-time responses to fire incidents.

One possible approach is to validate the SAR-derived outputs by incorporating ground truth data, such as information obtained from aerial infrared scanning, in-field surveys, or even crowd-sourced data. By comparing SAR imagery with in-situ observations and complementary datasets, the reliability and robustness of the results can be further strengthened. Integrating multiple data sources will create a more comprehensive and accurate picture of the bushfire situation, enabling better decision-making and response coordination.

Furthermore, future opportunities should also explore developing and implementing advanced algorithms and machine learning techniques to automate the processing and analysis of multiple source imagery. This automation would streamline the workflow and reduce the manual effort required for data interpretation and validation. By leveraging cutting-edge technologies, such as artificial intelligence and deep learning, it becomes possible to process large volumes of data efficiently and extract meaningful insights in near real-time.

In addition to technical advancements, future opportunities should also focus on building partnerships and collaborations with relevant stakeholders, including government agencies, emergency services, research institutions, and industry partners. These collaborations can facilitate data sharing, knowledge exchange, and the establishment of standardized protocols for data acquisition, processing, and validation. By fostering a collaborative environment, the bushfire management community can collectively work towards enhancing the confidence, reliability, and effectiveness of SAR-based monitoring and response systems.

Overall, future opportunities in the field of bushfire detection and monitoring should emphasize the processing of multiple source imagery and the verification of results through data integration and validation. By embracing technological advancements and fostering collaboration, we can unlock the full potential of SAR imagery and other data sources, revolutionizing how we respond to bushfires and minimizing the impacts on communities and ecosystems.

# References

Commonwealth of Australia (Geoscience Australia) (2023). https://digital.atlas.gov.au.

Ge, L., Y. Wang, Q. Zhang, Z. Du, C. Liu, Y. Dong, T. Sleigh, T. Guo, X. Lei and Z. Ma (2021). Quantitative, Near Real-Time Mapping of Bushfires Through Integration of Optical and SAR Remote Sensing Techniques. 2021 IEEE International Geoscience and Remote Sensing Symposium IGARSS.

Rahman, Z.-u., D. J. Jobson and G. A. Woodell (1996). Multi-scale retinex for color image enhancement. Proceedings of 3rd IEEE international conference on image processing, IEEE.

Sandwell, D., Mellors, R., Tong, X., Wei, M., & Wessel, P. (2011). Open radar interferometry software for mapping surface deformation, Wiley Online Library.

Zebker, H. A. and J. Villasenor (1992). Decorrelation in interferometric radar echoes. IEEE Transactions on Geoscience and Remote Sensing 30(5): 950-959.

Zhai, Y. and M. Shah (2006). Visual attention detection in video sequences using spatiotemporal cues. Proceedings of the 14th ACM international conference on Multimedia.